THE EUROPEAN
PHYSICAL JOURNAL D

Photonic crystal fiber-based plasmonic sensor with ITO for medical applications

Pibin Bing[a], Jiangfei Zhao, Qing Liu, Xiaohu Yi, Zhongyang Li, Hongtao Zhang, Zhiliang Chen, and Juan Xu

College of Electrical Engineering, North China University of Water Resources and Electric Power, Zhengzhou 450045, China

Abstract. In this paper, a photonic crystal fiber sensor is proposed for urine analysis of diabetic patients. Indium tin oxide (ITO) is adopted as plasmonic material to be coated on the polished plane to ensure a high flatness of the coating. The sensor is immersed in the liquid analyte for detection. Since the refractive index of the abnormal analyte is different from that of the normal level analyte, the change of its refractive index can be determined by comparing and analyzing the shifts of confinement loss peak shift. Simulation results show that the maximum wavelength sensitivity and resolution are 25,000 nm/RIU and 4×10^{-6} RIU in the refractive index detection range of 1.320–1.355. In addition, the sensor proposed in this paper can change the detection range and sensitivity by changing the thickness of ITO film, which means the thickness of ITO film can be optimized according to the application requirements to achieve customized PCF sensor. To sum up, the sensor proposed in this paper has potential applications in medical and chemical fields.

1 Introduction

In the past few decades, the photonic crystal fiber based on SPR has gradually become a new sensor that can be applied in medical, biological and chemical fields due to its advantages of flexible structure design and high sensitivity. In recent years, more and more researchers have carried out many researches and experiments on the combination of PCF-based sensors and applications. In 2012, Qi Liu et al. studied a tapered PCF refractive index (RI) sensor and the PCF sensor was immersed in the acetone and isopropanol mixtures of 20%, 40%, and 80% isopropanol, respectively [1]. The results showed that with the increase in the content of isopropanol, the transmission spectra presented a small redshift. This means that the PCF sensor can detect the changes of acetone and isopropanol content in the analyte; In 2017, Robinson et al. proposed a two-dimensional photonic crystal ring resonator-based sensor which is designed to detect the glucose concentration in urine [2]. The simulation results showed that the output energy intensity declined gradually while increasing the glucose concentration in urine. This study proved that the urine of diabetic patients was different from the normal level and that glucose concentration was positively correlated with RI. In 2021, Shakya et al. proposed a PCF sensor that used Au and TiN as plasmonic materials for

measuring moisture content in transformer oil [3]. Simulation results showed that the maximum wavelength sensitivity of the sensor is 11000 nm/RIU. The experiment results showed that the sensor has a strong discrimination ability of water and oil. This means that PCF sensor also has the application potential of detecting water content in acetone. In 2021, Guo Zhu et al. developed a biosensor for the detection of the ACh biomolecule [4]. Gold nanoparticles and MoS_2 nanoparticles are used to enhance the sensor probe's sensing ability and biocompatibility. This study has implications for the application of SPR effect in diabetes monitoring. Inspired by the above studies, this paper proposes a sensor based on SPR-PCF, which has application prospect in urine test of diabetic patients.

According to the International Diabetes Federation (IDF), about 537 million people (aged 21–79) are affected by diabetes in 2021 and the number of people with diabetes is expected to reach 643 million by 2030, and 783 million by 2045 [5]. The number of diabetic patients in China ranks first in the world. There are an estimated 140 million adults with diabetes in China, accounting for 26% of the world's diabetes population. Blindness, kidney failure, heart attack, stroke and lower extremity amputations can accompany diabetes [6]. Access to insulin may be limited in some countries, especially in economically disadvantaged households. This, combined with the lack of access to self-care tools, including structured diabetes education, often leads to

[a] e-mail: bing463233@163.com (corresponding author)

severe disability and premature death as harmful substances called ketones build up in the body, leading to diabetic ketoacidosis (DKA) [5]. One of the hallmarks of diabetic ketoacidosis (DKA) is the accumulation of acetoacetate (AcAc), beta-hydroxybutyrate (β-OHB) and acetone in body fluid [7].

However, acetone can be excreted through breath and urine and metabolized in the body. The RI of the urine is varied, if the glucose concentration presented in the urine is varied, as shown in Table 1 [8, 9]. In addition, acetone is a flammable and harmful chemical substance, PCF sensor is suitable for daily monitoring of acetone and detecting moisture content in acetone because it is not driven by electricity.

ITO thin film is a highly degenerate n-type semiconductor material with high electrical conductivity, high visible light transmittance, high mechanical hardness and good chemical stability. ITO is a metal oxide that can cause its own refractive index to decrease by increasing the Sn dopant in the target and/or increasing the deposition temperature—which increases the electron density in the film. The plasma wavelength of the ITO film can also be controlled, thanks to the fact that the doping level in the target and the deposition temperature can be determined on demand [10]. These characteristics of ITO will affect parameters such as the detection range and sensitivity of the sensor, and also change the operating wavelength of the sensor. These excellent characteristics of ITO will undoubtedly endow the sensor with better performance.

In this paper, a SPR-based D-shaped PCF sensor is proposed. ITO is deposited on the polished plane as a plasmonic material, and the thickness of ITO film is 40 nm. The selection of a single ITO material not only improves the specificity of the sensor for the monitoring of diabetes, but also reduces the difficulty of coating compared with sensors coated with multiple plasmonic materials. Since the RI of water and acetone near 1600 nm is about 1.320 and 1.355, the RI detection range of the sensor is set as 1.320–1.355. Simulation results show that the maximum wavelength sensitivity and resolution are 25,000 nm/RIU and 4×10^{-6} RIU, respectively. The sensor has a simple structure, which can be applied to different fields by changing the thickness of ITO material. It has a potential application in urine test and daily monitoring of diabetes patients thanks to a high sensitivity and simple detection method.

2 Structure and theoretical modeling

The cross section of the PCF sensor proposed in this paper is shown in Fig. 1. The structure of PCF is composed of air holes arranged in an equilateral triangle. The air holes in the center of the optical fiber and the two air holes above are small and used to form the fiber core. The microchannels on both sides of ITO film consist of half of two large air holes. In order to achieve

the RI detection range of sensor 1.320–1.355, the diameter and spacing of the three air holes were optimized as $d_1 = 0.6\ \mu m$, $d_2 = 1\ \mu m$, $d_3 = 2.6\ \mu m$, $\Lambda = 2\ \mu m$, respectively. The thickness of ITO film is t = 40 nm, and the thickness of perfect match layer (PML) is $2\ \mu m$. Additionally, the optical fiber is $16\ \mu m$ in diameter.

The proposed sensor uses fused silica as background material, and the refractive index of fused silica is given by Sellmeier equation [11]:

$$n_{\mathrm{SiO_2}}^2(\lambda) = 1 + \frac{A_1 \lambda^2}{\lambda^2 - B_1} + \frac{A_2 \lambda^2}{\lambda^2 - B_2} + \frac{A_3 \lambda^2}{\lambda^2 - B_3} \quad (1)$$

where λ is the wavelength of the incident light, $A_1 = 0.696166300$, $A_2 = 0.407942600$, $A_3 = 0.897479400$, $B_1 = 4.67914826 \times 10^{-3} \mu m^2$, $B_2 = 1.35120631 \times 10^{-2} \mu m^2$, $B_3 = 97.9340025\ \mu m.^2$. The dielectric constant of ITO is given by Drude model [12]:

$$\varepsilon_m(\lambda) = \varepsilon_\infty - \frac{\lambda^2 \lambda_c}{\lambda_p^2 (\lambda_c + i\lambda)} \quad (2)$$

Here, ε_∞ is the dielectric constant for the infinite value of the frequency of ITO and whose value is 3.80. $\lambda_p = 5.6497 \times 10^{-7}$ m and $\lambda_c = 11.21076 \times 10^{-6}$ m. They are the plasmonic and collision wavelengths of ITO, respectively.

The finite element method (FEM) is used to numerically analysis. The PML is used as the boundary condition to absorb the transitory field dispersed. The confinement loss of the core mode and SPP mode is calculated by following equation [13]:

$$\alpha_{\mathrm{loss}}(dB/m) = 40\pi \frac{\mathrm{Im}(n_{\mathrm{eff}})}{\ln(10)\lambda} \quad (3)$$

where λ is wavelength in meter, $\mathrm{Im}(n_{\mathrm{eff}})$ is the imaginary part of the effective mode RI.

3 Simulation and analysis

The dispersion relationship between core-guide mode of y-polarized and SPP mode is shown in Fig. 2. The black and blue curves in the figure represent the real part of the effective refractive index of the y-polarized core-guided mode and SPP mode, respectively. When the wavelength increases from 1500 to 1725 nm, the two curves decline simultaneously at the beginning. When the wavelength is 1578 nm, the two curves cross and the imaginary part of the effective index of the core mode reaches its maximum. At this time, the core-guided mode and SPP mode have strong coupling and the loss reaches the maximum [14]. As the wavelength continues to increase, the energy of the core-guided mode and the SPP mode convert to each other [15]. The entire coupling process of SPP mode and core-guide mode can be seen in insets. Insets (b), (e), (a), (f) show the energy field distribution of core-guided mode of y-polarized

Table 1 Glucose concentration in urine and its RI

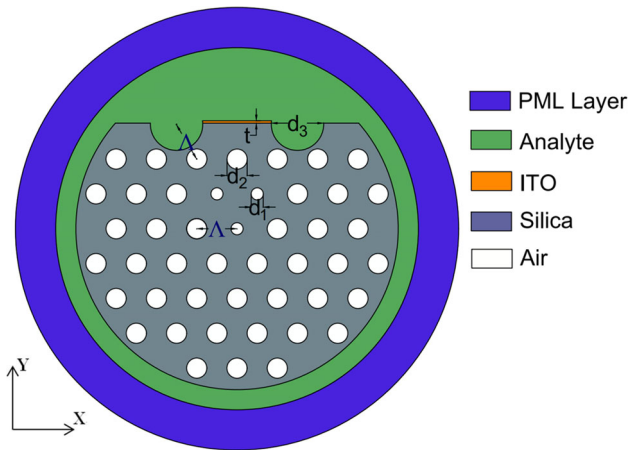| Glucose concentration in urine	Normal (0 mg/dl–15 mg/dl)	0.625 gm/dl	1.25 gm/dl	2.5 gm/dl	5 gm/dl	10 gm/dl
RI	1.335 ± 0.001	1.336 ± 0.001	1.337 ± 0.001	1.338 ± 0.001	1.341 ± 0.001	1.347 ± 0.001

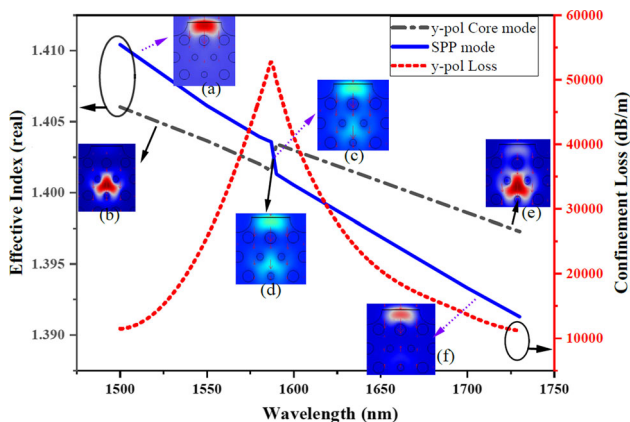**Fig. 1** Cross section of proposed sensor

Fig. 2 Dispersion relationship of the y-polarized core mode and SPP mode. Energy field distribution of **a** SPP mode **b** y-polarized core mode **c** SPP mode **d** core mode **e** core mode **f** SPP mode ($n = 1.325$)

Fig. 3 Confinement loss spectra for analyte RI range from 1.320 to 1.355

and SPP mode at 1500 nm and 1730 nm. Insets (d) and (c) show that the core-guided mode and SPP mode are coupled strongly at 1578 nm. The energy field distribution of the core-guide mode and SPP mode is almost the same. Due to the obvious coupling between the core-guided mode of y-polarized and SPP mode, the core-guided mode of y-polarized is chosen in the analysis of the sensor characteristics.

The confinement loss spectra of the sensor proposed in this paper in the RI range of 1.320–1.355 are shown in Fig. 3. With the increase in RI of the analyte, the phase matching point of the core-guided mode and SPP mode is redshifted, and the loss spectra of the sensor
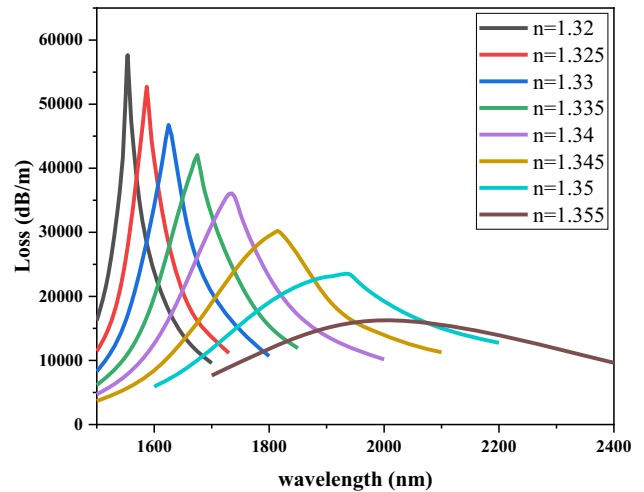
are redshifted. When the RI of the analyte is 1.320, the maximum loss peak is 5.2718×10^4 dB/m. With the increase in RI, the coupling intensity of core-guided mode and SPP mode decreases, and the loss peak gradually declines to 1.6245×10^4 dB/m of RI = 1.355.

One of the most important parameters of the SPR sensor is the wavelength sensitivity (WS), which can be expressed as follows [16]:

$$S_\lambda(\text{nm/RIU}) = \Delta\lambda_{\text{peak}}/\Delta n_a \qquad (4)$$

where $\Delta\lambda_{\text{peak}}$ is the peak wavelength shift and Δn_a is the RI variation in the analyte. As shown in Fig. 3, $\Delta\lambda_{\text{peak}}$ is 33 nm, 40 nm, 48 nm, 61 nm, 81 nm, 125 nm and 64 nm for the analyte RI from 1.320 to 1.350. The corresponding WS is 6600 nm/RIU, 8000 nm/RIU, 9600 nm/RIU, 12200 nm/RIU, 16200 nm/RIU, 25000 nm/RIU, and 12800 nm/RIU, respectively. The maximum WS and average WS are 25,000 nm/RIU and 12,914 nm/RIU, respectively.

Sensor resolution is a parameter that is used to measure the lowest change of analyte RI that can be detected by the sensor. The sensor resolution can be defined as [17, 18]:

$$R(\text{RIU}) = \Delta n_a \times \Delta\lambda_{\text{min}}/\Delta\lambda_{\text{peak}} \qquad (5)$$

where Δn_a is the variation in the analyte RI, $\Delta\lambda_{\text{min}}$ is the minimum spectral resolution, and $\Delta\lambda_{\text{peak}}$ is the shift of resonance wavelength.
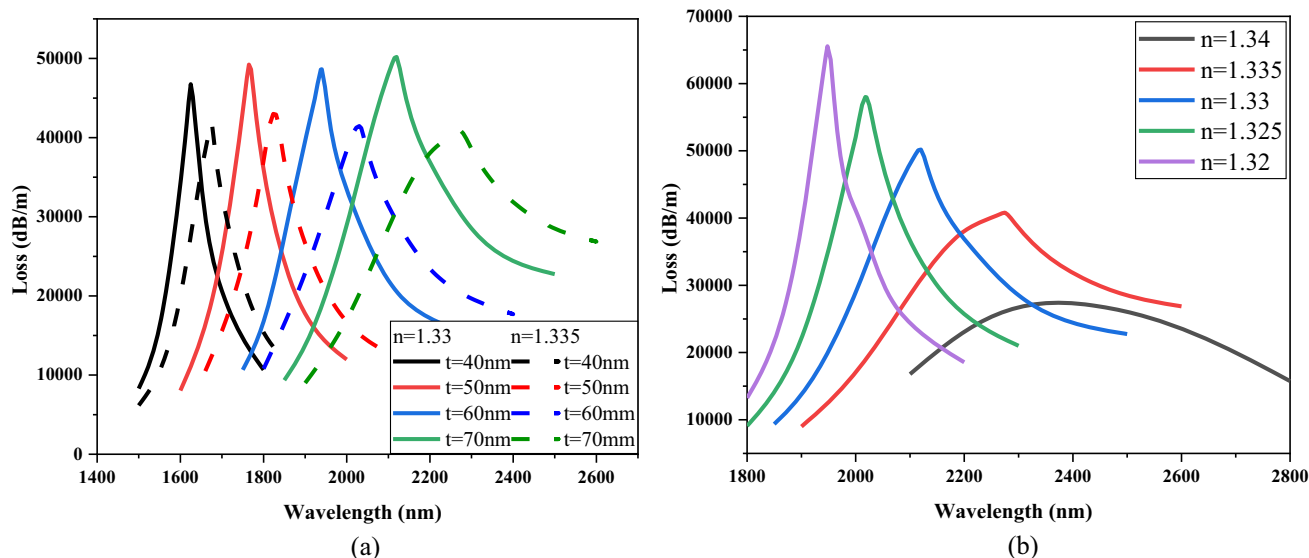
Fig. 4 **a** Confinement loss spectra of the sensor with different thickness of ITO layer for RI of 1.330 and 1.335. **b** Confinement loss spectra of the sensor with thickness of ITO layer for 70 nm

Table 2 Sensing performance of the sensor for different analyte RI

Analyte RI	CL($\times 10^4$ dB/m)	Peak wavelength (nm)	Peak shift (nm)	WS (nm/RIU)	Resolution (RIU)
1.320	5.9456	1554	33	6600	1.52×10^{-5}
1.325	5.2718	1587	40	8000	1.25×10^{-5}
1.330	4.7564	1627	48	9600	1.04×10^{-5}
1.335	4.2291	1675	61	12,200	8.20×10^{-6}
1.340	3.6687	1736	81	16,200	6.17×10^{-6}
1.345	3.0306	1817	125	25,000	4×10^{-6}
1.350	2.3437	1942	64	12,800	7.81×10^{-6}
1.355	1.6245	2006	N/A	N/A	N/A

When the RI of the analyte is 1.345, the resolution of the sensor can reach 4×10^{-6} RIU. In addition, various parameters of the sensor under different RIs are summarized in Table 2.

Figure 4a illustrates the confinement loss spectra for different ITO film thickness. It can be seen that the thickness of ITO film plays a key role in the resonance wavelength of the sensor. As the thickness of ITO film increases from 40 to 70 nm, the loss peak shifts from 1625 to 2120 nm, while the resonance intensity changes little. The thickness of ITO film also has great influence on the sensitivity and analyte RI range. As can be seen from Fig. 4a, when the thickness of ITO film increases from 40 to 70 nm, $\Delta\lambda_{\text{peak}}$ of the sensor is 50 nm, 65 nm, 90 nm and 155 nm for the analyte RI = 1.330. The corresponding wavelength sensitivity varies from 10000 nm/RIU, 13,000 nm/RIU, 18,000 nm/RIU to 30,100 nm/RIU, which means that the increase in ITO film thickness greatly improves the sensitivity. Figure 4b shows the confinement loss spectra of the sensor when the thickness of ITO film is 70 nm. The maximum wavelength sensitivity is 30100 nm/RIU for the analyte RI range of 1.320–1.340. From Fig. 4a and b,

it can be concluded that with the increase in ITO film thickness, the sensitivity of sensor is improved while the RI range of analyte is also get narrow. The analyte RI range of the sensor can be changed by depositing ITO films with different thicknesses according to different application scenarios. In order to better realize the analyte RI range of 1.320–1.355, so as to realize the application of sensor in urine test of diabetic patients, the thickness of ITO film is set as t = 40 nm.

Figure 5 shows the influence of the microchannel diameter on the confinement loss spectra for RIs of 1.330 and 1.335. As can be seen from Fig. 5, with the decrease in microchannel diameter, the resonance peak red-shifted and the resonance intensity becomes weak. As the diameter of the microchannel decreases from 2.6 μm to 1.4 μm, the passway between the fiber core and ITO film becomes larger. As the wavelength increases, the coupling intensity between the core-guided mode and SPP mode becomes weaker, the loss peak red-shifted, and the energy between the core-guided mode and SPP mode reduces and the coupling intensity becomes weaker. As the diameter of the microchannel decreases from 2.6 μm to 1.4 μm, $\Delta\lambda_{\text{peak}}$
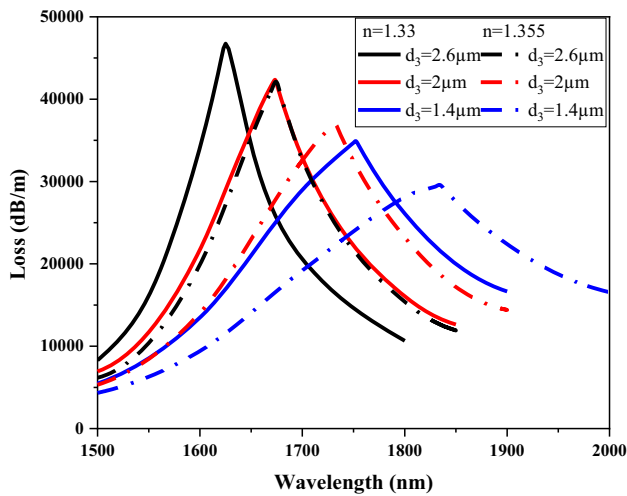
Fig. 5 Confinement loss spectra of the sensor with different diameter of microchannel

of the sensor at n = 1.330 is 50 nm, 59 nm, 82 nm, respectively. It can be inferred from the above that the introduced microchannel further weakens the cladding's ability to bind electromagnetic waves, and the energy is more concentrated in the core, which improves the coupling strength between the core-guided mode and the SPP mode to a certain extent. Furthermore, it is not difficult to infer from the changing law of the curves that the smaller the diameter of the microchannel, the smaller the analyte RI range, and the wavelength sensitivity also has a small increase. In order to better realize the RI detection range of 1.320–1.355, the diameter of the microchannel (d_3) was set to 2.6 μm.

Figure 6 depicts the spectra of different air hole diameters (d_1). As the d_1 increases from 0.6 μm, 0.65 μm to 0.7 μm, the loss peak declines gradually, which indicating that the smaller d_1 provides a larger light field

and more energy is confined to the fiber core. With the increase in d_1, the light field gradually shrinks, the energy in the fiber core declines, and fewer photons react with the free electrons of ITO film so that the SPR phenomenon is weaker. As can be seen from Fig. 6b, when the diameter of the air hole increases from 0.6 μm to 0.7 μm, the corresponding wavelength sensitivity of the sensor is 10000 nm/RIU, 12,400 nm/RIU, and 21,000 nm/RIU for the analyte RI range of 1.330–1.335. In addition, we found in the calculation that when the analyte RI range of 1.345–1.350, the wavelength sensitivity is 25000 nm/RIU for the d_1 is 0.6 μm. When d_1 is 0.65 μm and 0.7 μm, the sensor cannot achieve normal detection when the refractive index exceeds 1.345. From Fig. 6a and b, it can be concluded that with the increase in diameter of the air hole (d_1), the sensitivity of sensor is improved while the RI range of analyte is also get narrow. In order to better realize the RI detection range of 1.320–1.355, the diameter d_1 was set to 0.6 μm.

Table 3 shows the performance comparison between the SPR-PCF sensor proposed in this article and the existing SPR-PCF sensors [19, 20] in a similar refractive index detection range. As can be seen, the proposed sensor has a higher wavelength sensitivity and a lower resolution in a similar detection range.

The proposal and successful fabrication of photonic crystal fiber provide a new research platform for fiber SPR immune sensing [21, 22]. Due to the flexible structural design and unique light guiding mechanism of PCF, its optical properties can be effectively adjusted by changing the shape, size and distribution of the internal air holes, which solves the problem of phase matching between the core mode and the plasma mode of the ordinary optical fiber SPR sensor [23, 24]. At present, the drawing process for this type of PCF is relatively mature, and some D-type PCFs have appeared on the market. So, we can use femtosecond laser drilling
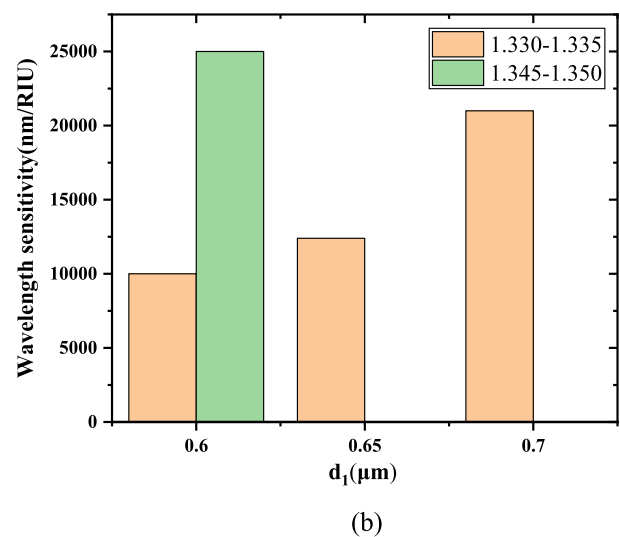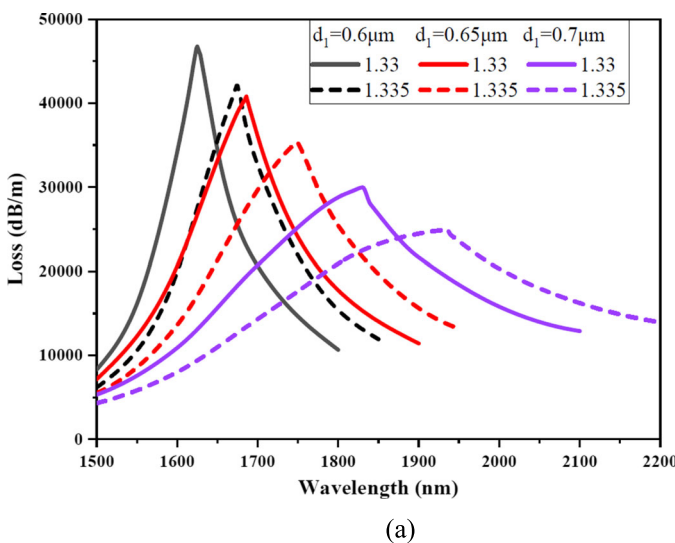

(a)

(b)

Fig. 6 a Confinement loss spectra of the sensor with different diameter of d_1. **b** Wavelength sensitivity of the sensor with different diameter of d_1

Table 3 Comparison of the proposed SPR-PCF sensor with existing SPR-PCF sensors

Reference	Detection range	Plasmonic material	Max RI sensitivity (nm/RIU)	Resolution (RIU)
3	1.33–1.34	Au and TiN	11,000	9.09×10^{-6}
9	1.338–1.358	Au	2500	1.754×10^{-5}
18	1.31–1.40	Au	6000	1.66×10^{-5}
19	1.33–1.37	ITO	5200	1.92×10^{-5}
20	1.33–1.36	Ag and Au	12,400	8.06×10^{-6}
This senor	1.320–1.355	ITO	25,000	4×10^{-6}

for the air holes inside the optical fiber [25], and magnetron sputtering for the coating of plasma materials [26]. So, the structure we have designed is feasible.

4 Conclusion

A SPR-PCF sensor coated with ITO film is proposed and analyzed numerically in this paper. By optimizing the structure parameters, the sensor has good performance in the analyte RI range of 1.320–1.355. The maximum wavelength sensitivity and the sensor resolution can reach 25,000 nm/RIU and 4×10^{-6} RIU, respectively. In addition, the sensor can be applied to different application scenarios by changing structure parameters. For example, the sensor can detect analyte with lower RI by increasing the thickness of ITO film. Thanks to its simple structure, the sensor is easy to fabricate and can be manufactured using existing technology. Because of its excellent performance, the sensor proposed in this paper has a broad application prospect in the detection of moisture content in acetone and diabetes urine test.

Author contributions

All the authors were involved in the preparation of the manuscript. All the authors have read and approved the final manuscript.

Data availability statement "This manuscript has no associated data or the data will not be deposited. [Authors' comment: Data may be obtained from the authors upon reasonable request.]

Declarations

Conflict of interest The authors declare that they have no known competing financial interests or personal relationships that could have appeared to influence the work reported in this paper.

References

1. Q. Liu, Q. Wang, Refractive index sensor based on tapered PCF in-line interferometer. Chin. Opt. Lett. **10**(9), 090601–090601 (2012)
2. S. Robinson, N. Dhanlaksmi, Photonic crystal based biosensor for the detection of glucose concentration in urine. Photonic Sens. **7**(1), 11–19 (2017)
3. A.K. Shakya, S. Singh, Design of novel Penta core PCF SPR RI sensor based on fusion of IMD and EMD techniques for analysis of water and transformer oil. Measurement **188**, 110513 (2022)
4. G. Zhu, Y. Wang, Z. Wang, R. Singh, C. Marques, Q. Wu, B.K. Kaushik, R. Jha, B.Y. Zhang, S. Kumar, Localized plasmon-based multicore fiber biosensor for acetylcholine detection. IEEE T Instrum. Meas. **71**, 1–9 (2022)
5. IDF Diabetes Atlas 10th edition, Available online: www.diabetesatlas.org, 2021
6. World Health Organization, Newsroom/Fact sheets/Detail/Diabetes, Available online: https://www.who.int/news-room/fact-sheets/detail/diabetes, 2021
7. O.E. Owen, V.E. Trapp, C.L. Skutches, M.A. Mozzoli, R.D. Hoeldtke, G. Boden, G.A. Reichard Jr., Acetone metabolism during diabetic ketoacidosis. Diabetes **31**(3), 242–248 (1982)
8. P. Sharma, P. Sharan, Design of photonic crystal-based biosensor for detection of glucose concentration in urine. IEEE Sens. J. **15**(2), 1035–1042 (2015)
9. M.E. Rahaman, R.H. Jibon, M.S. Ahsan, F. Ahmed, I.B. Sohn, Glucose level measurement using photonic crystal fiber-based plasmonic sensor. Plasmonics **17**(1), 1–11 (2022)
10. H. Kim, C. Gilmore, A. Piqué, J. Horwitz, H. Mattoussi, H. Murata, Z. Kafafi, D. Chrisey, Electrical, optical, and structural properties of indium–tin–oxide thin films for organic light-emitting devices. J. Appl. Phys. **86**(11), 6451–6461 (1999)

11. P.B. Bing, J.L. Sui, G.F. Wu, X.Y. Guo, Z.Y. Li, L. Tan, J.Q. Yao, Analysis of dual-channel simultaneous detection of photonic crystal fiber sensors. Plasmonics **15**(4), 1071–1076 (2020)

12. A. Patnaik, K. Senthilnathan, R. Jha, Graphene-based conducting metal oxide coated D-shaped optical fiber SPR sensor. IEEE Photonic Tech. L **27**(23), 2437–2440 (2015)

13. Q.L. Wu, Y. Zhao, Y.N. Zhang, Y. Yang, Characteristics of a new multi-channel sensing device based on C-type photonic crystal fibers. Opt. Laser Technol. **134**, 106622 (2021)

14. Z. Yang, L. Xia, C. Li, X. Chen, D.M. Liu, A surface plasmon resonance sensor based on concave-shaped photonic crystal fiber for low refractive index detection. Opt. Commun. **430**, 195–203 (2019)

15. X. Chen, L. Xia, C. Li, Surface plasmon resonance sensor based on a novel D-shaped photonic crystal fiber for low refractive index detection. IEEE Photonics J. **10**(1), 1–9 (2018)

16. W. Liu, C.J. Hu, L. Zhou, Z. Yi, Y. Shi, C. Liu, J.W. Lv, L. Yang, P. Chu, A highly sensitive D-type photonic crystal fiber infrared sensor with indium tin oxide based on surface plasmon resonance. Mod. Phys. Lett. B **36**(01), 2150499 (2022)

17. Q. Liu, Y. Jiang, Y.D. Sun, C.J. Hu, J.D. Sun, C. Liu, J.W. Lv, J. Zhao, Z. Yi, P.K. Chu, Surface plasmon resonance sensor based on U-shaped photonic quasi-crystal fiber. Appl. Optics **60**(6), 1761–1766 (2021)

18. M. Kiroriwal, P. Singal, Numerical investigation of gold plated single-core photonic crystal fiber-based refractive index sensor. Int. J Mod. Phys. B **36**(01), 2250010 (2022)

19. J.N. Dash, R. Jha, Highly sensitive D shaped PCF sensor based on SPR for near IR. Opt. Quant. Electron. **48**, 1–7 (2016)

20. C. Liu, J. Wang, X. Jin, F. Wang, L. Yang, J. Lv et al., Near-infrared surface plasmon resonance sensor based on photonic crystal fiber with big open rings. Optik **207**, 164466 (2020)

21. J.C. Knight, Photonic crystal fibres. Nature **424**(6950), 847–851 (2003)

22. P. Russell, Photonic crystal fibers. Science **299**(5605), 358–362 (2003)

23. Y. Zhao, Z.Q. Deng, J. Li, Photonic crystal fiber based surface plasmon resonance chemical sensors. Sens. Actuators, B Chem. **202**, 557–567 (2014)

24. A.A. Rifat, R. Ahmed, A.K. Yetisen et al., Photonic crystal fiber based plasmonic sensors. Sens. Actuators, B Chem. **243**, 311–325 (2017)

25. I. South, Novel D-type fiber optic localized plasmon resonance sensor realized by femtosecond laser engraving. J. Laser Micro/Nanoeng. **5**, 1–5 (2010)

26. X.-Q. Tan, J.-Y. Liu, J.-R. Niu, J.-Y. Liu, J.-Y. Tian, Recent progress in magnetron sputtering technology used on fabrics. Materials **11**(10), 1953 (2018)